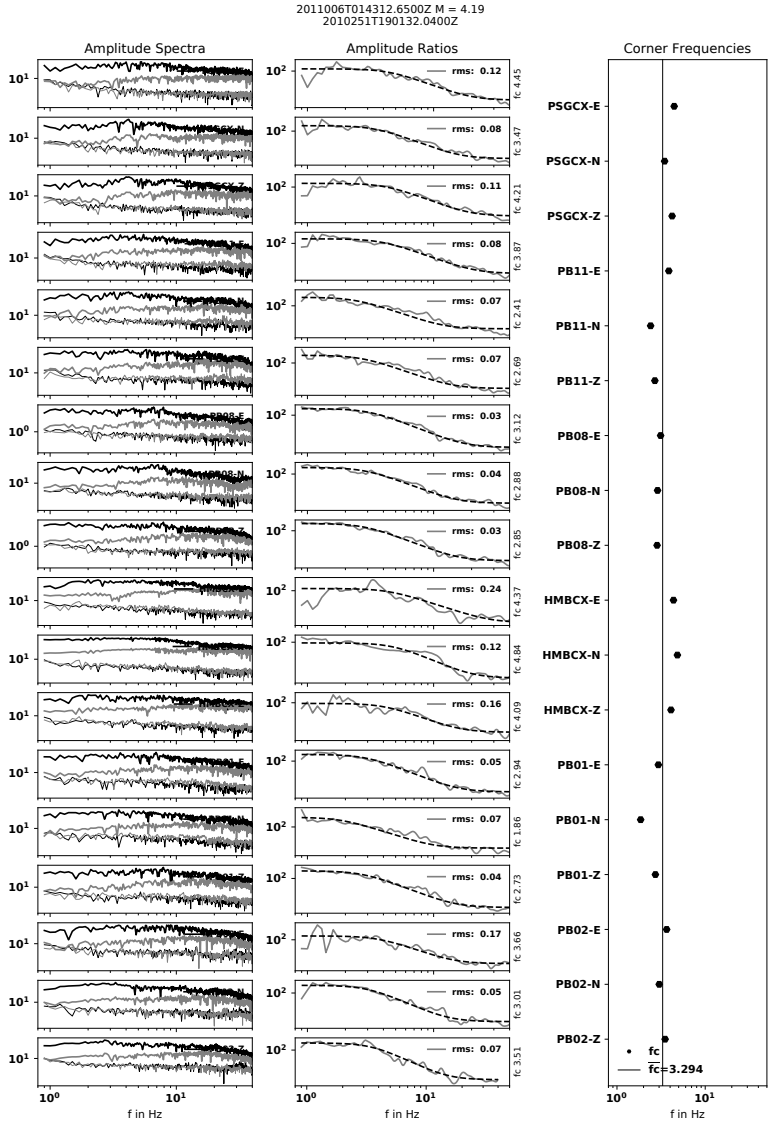

Figure S 14: P wave velocity spectra, spectral ratios and estimated corner frequencies for one more exemplary event.

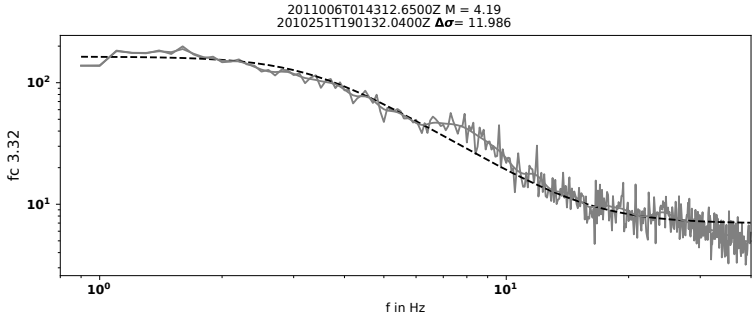

Figure S 15: Corresponding average velocity spectrum for the event from Figure S 14.

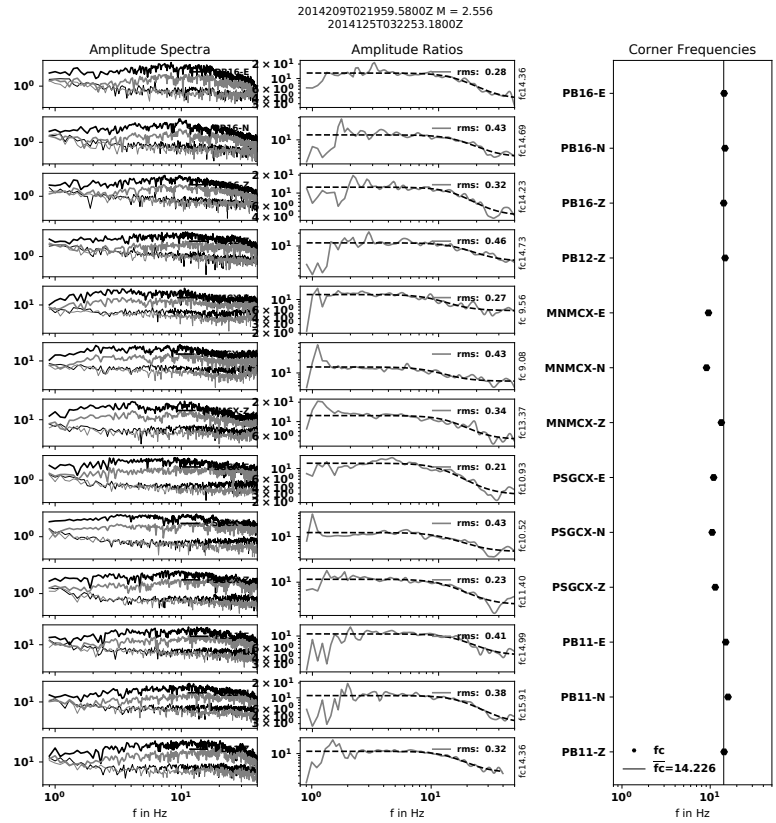

Figure S 16: P wave velocity spectra, spectral ratios and estimated corner frequencies for one more exemplary event.

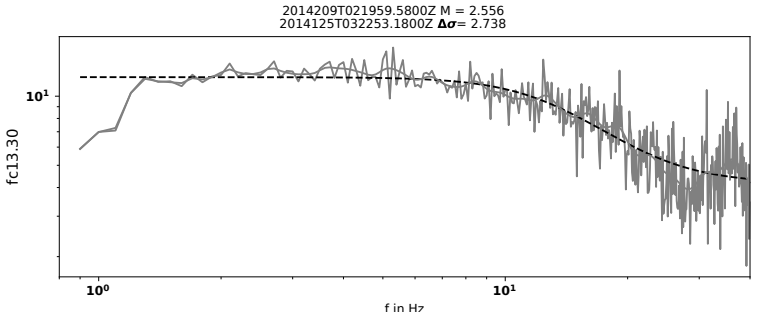

Figure S 17: Corresponding average velocity spectrum for the event from Figure S 16.

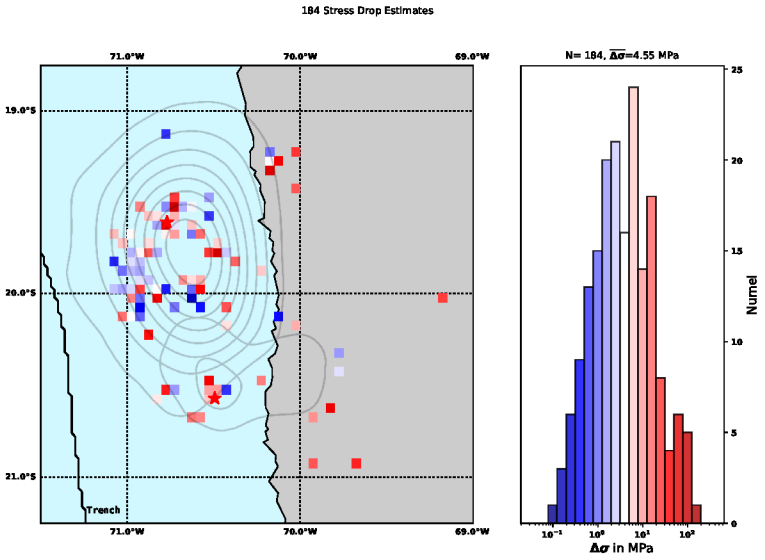

Figure S 18: Stress drop distribution averaged on a regular grid, similar to Figure 8 but showing only events that occurred **before the main Iquique event.**

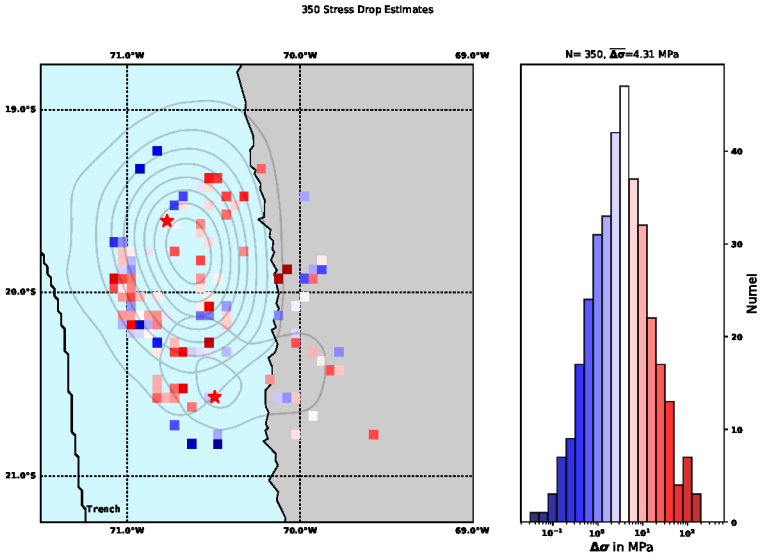

Figure S 19: Stress drop distribution averaged on a regular grid, similar to Figure 8 but showing only events that occurred **after the main Iquique event.**

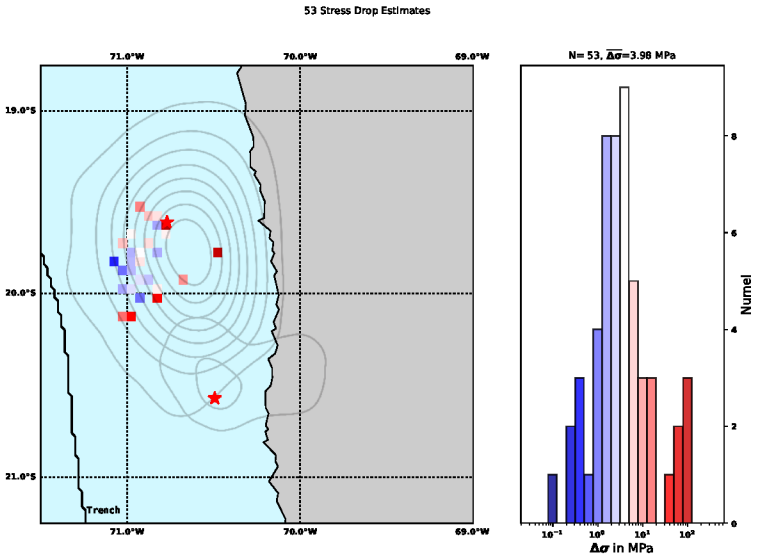

Figure S 20: Stress drop distribution averaged on a regular grid, similar to Figure 8 but showing only events that occurred **in the two weeks before the main Iquique event.**

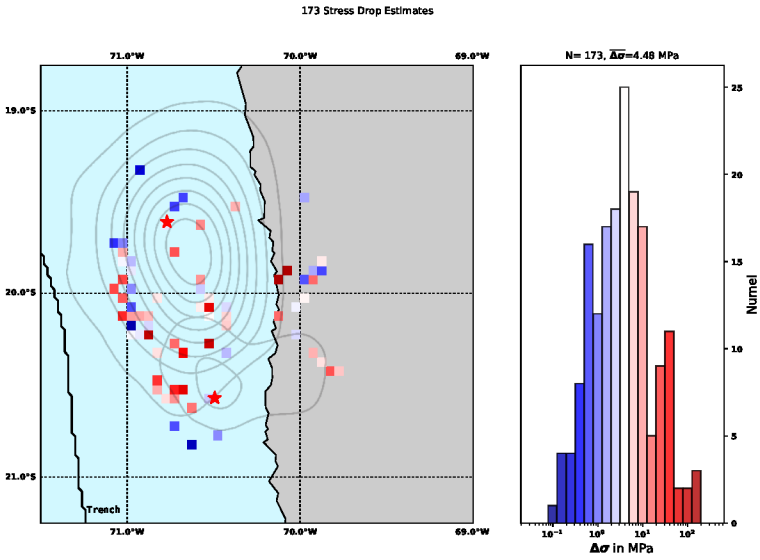

Figure S 21: Stress drop distribution averaged on a regular grid, similar to Figure 8 but showing only events that occurred **in the four weeks after the main Iquique event.**

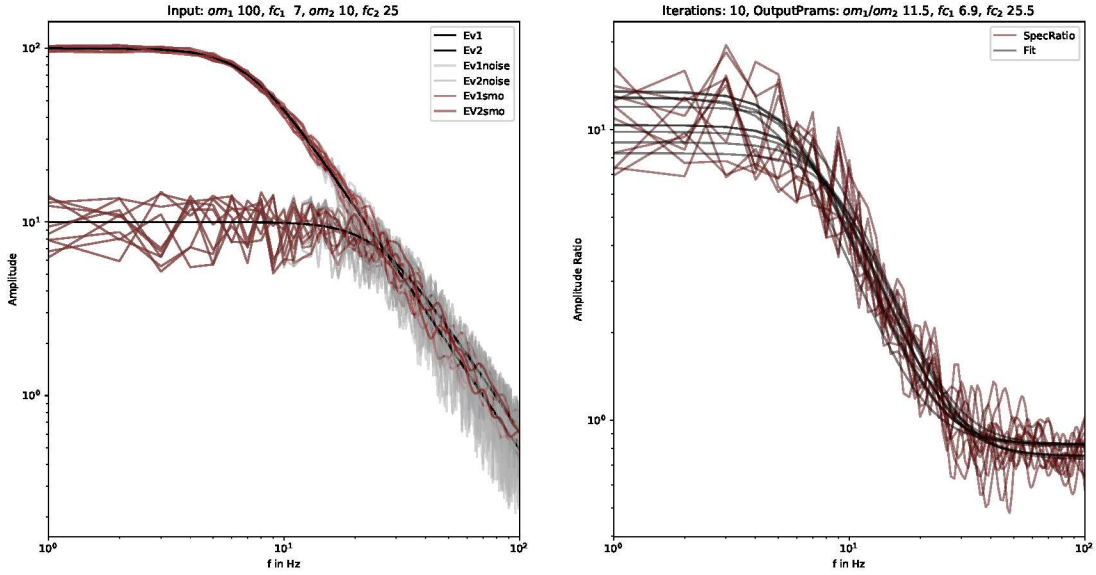

Figure S 22: Influence of smoothing [Konno and Ohmachi, 1998] on the estimated corner frequency. Displayed are ten realizations of the test. On the left, the input spectra (black), the spectra with noise (grey) and the smoothed spectra (brown) of the target and of the EGF event are shown. On the right, the corresponding spectral ratios are shown with their fits, respectively. The input and output parameters are displayed above the plots. The smoothing operator has only a minimal impact on the decrease of the estimated corner frequency. We conclude that it is reasonable to use the smoothing to stabilize the spectral ratio approach with the real data.

Influence of Smoothing on the Corner Frequency Estimates

We test the influence of the Konno-Omachi smoothing on the estimated corner frequency. For this, the spectra of an EGF pair are simulated using the Boatwright spectral model with input parameters $\Omega_1, fc_1, \Omega_2, fc_2$ in the range of typical values from the real data. White random noise is added such that the noise amplitude is stable over all frequencies. Noise range is ± 0.5 times the model amplitude of the smaller event. The spectra are then smoothed using the Konno- Ohmachi smoothing function from Obspy, an implementation of the approach of Konno and Ohmachi, 1998. Next, the ratio of the two spectra is computed and the data is fitted using the trust region reflective method from scipy curve_fit. In Figure S 22, ten exemplary event pair curves are shown. The procedure is iterated for different fc_1 values with 1000 runs for each tested

corner frequency. The results, shown in Table S 1, demonstrate that the input parameters are recovered reliably. The standard deviation values are in the range of 15%. A minimal systematic shift towards smaller values for fc_1 is seen. We conclude that the smoothing is applicable.

fc_{in}	fc_{out}	fc_{std}
4	4.0	0.7
7	6.9	0.9
10	9.8	1.2
14	13.5	1.9

Table S 1: Results of synthetic smoothing tests for 1000 iterations using varying input values for the corner frequency fc_1 in Hz. All other inputs are fixed ($\Omega_1 = 100, fc_1 = var, \Omega_2 = 10, fc_2 = 25$).

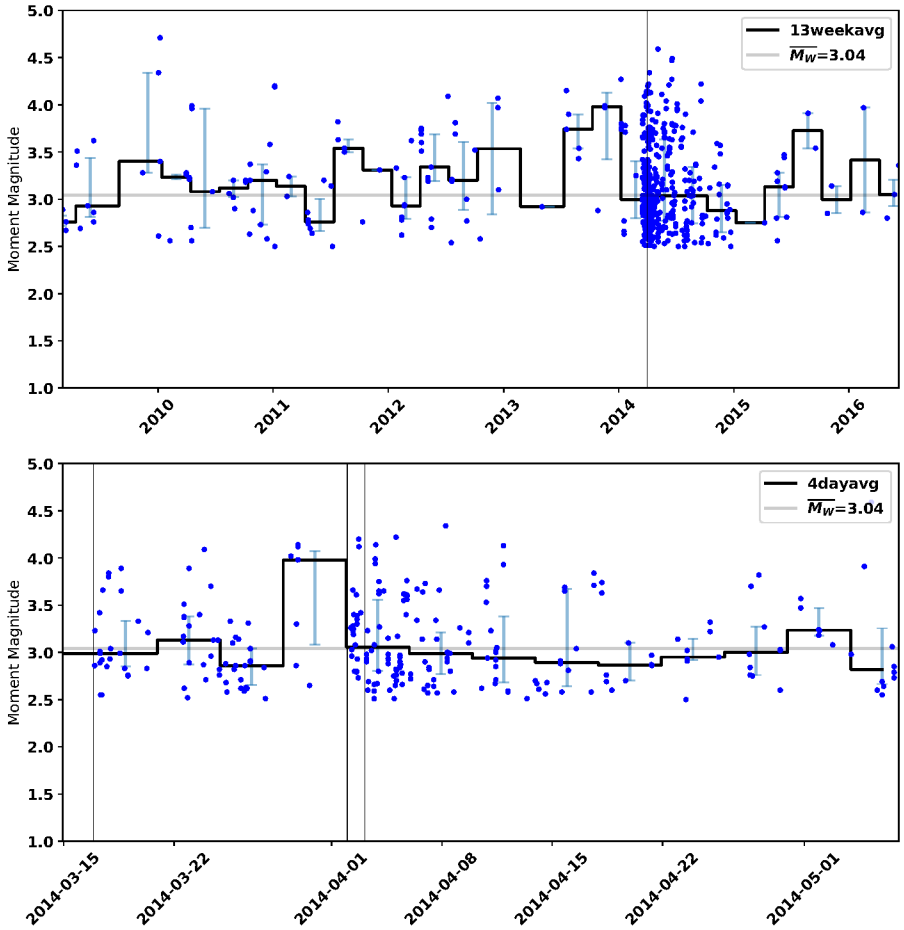

Figure S 23: Variation of event magnitude with time. The figure shows the same time intervals as used for the temporal stress drop variation (Figure 10 main manuscript). The three vertical grey lines in the bottom panel denote the origin times of the M_W6.6 foreshock, the M_W8.1 mainshock, and the M_W7.6 aftershock. In both panels the median magnitude of the entire result ensemble (M_W = 3.04) is underlain as a grey line. Note the principally similar behavior of the curves compared to the stress drop curves in Figure 10 of the main manuscript. The shapes of the two curves show similarity indicating a correlation of event moment magnitude and stress drop which is substantiated in Figure 11 of the main manuscript.

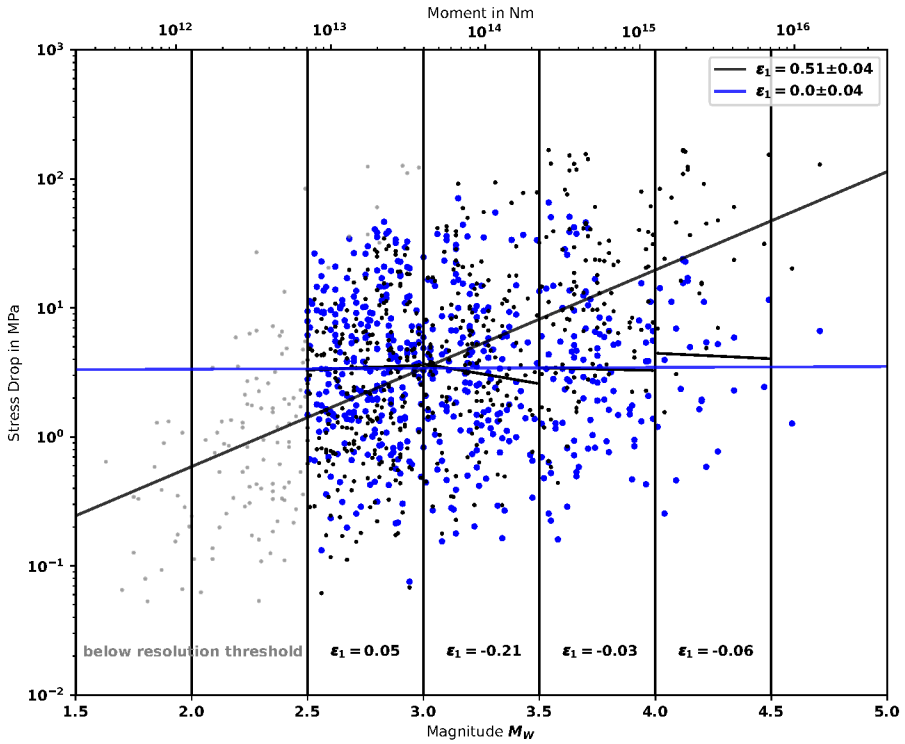

Figure S 24: Scaling of stress drop with seismic moment. The black line and dots are the original values as depicted in Figure 11. Using a linear regression the gradient of ε_1=0.51 was estimated (black line, see main manuscript). Blue dots show stress drops with a removed gradient, i.e., a forced removal of moment dependency. The regression then yields ε_1=0 (blue line). By producing such a corrected data set we are able to test, if the spatio-temporal variability (Figures S 25 and S 26) is based predominantly on moment variability or is a separate signature.

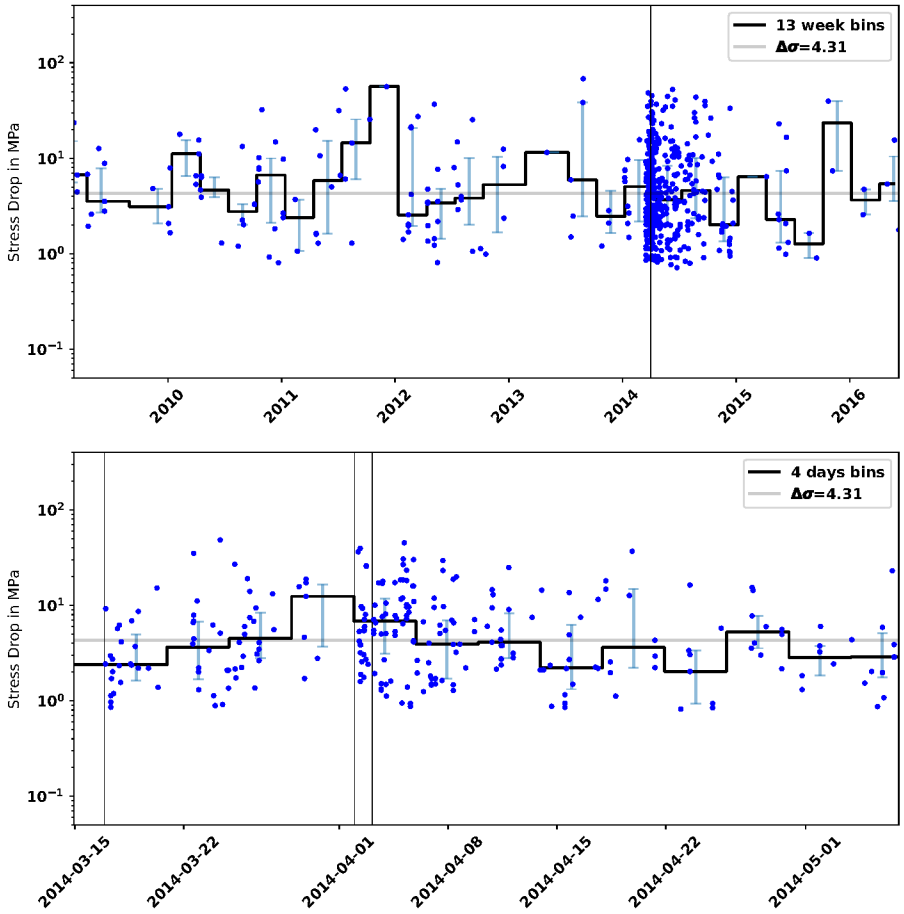

Figure S 25: Stress drop variation with time similar to Figure 10. The moment dependency of the stress drop values was removed as explained in Figure S 24 in order to test if the temporal variability of stress drop is caused by variations of the seismic moment distribution. Note that the overall stress drop variation pattern remains similar to the original results in Figure 10. For example, we recognise a rise of stress drop values prior to the Iquique mainshock (bottom plot, second vertical line) and a gradual decrease afterwards. The range of variability, however, is decreased, indicating that a coinciding effect of both stress drop variation and moment variation are present to obtain the original stress drop variability from Figure 10.

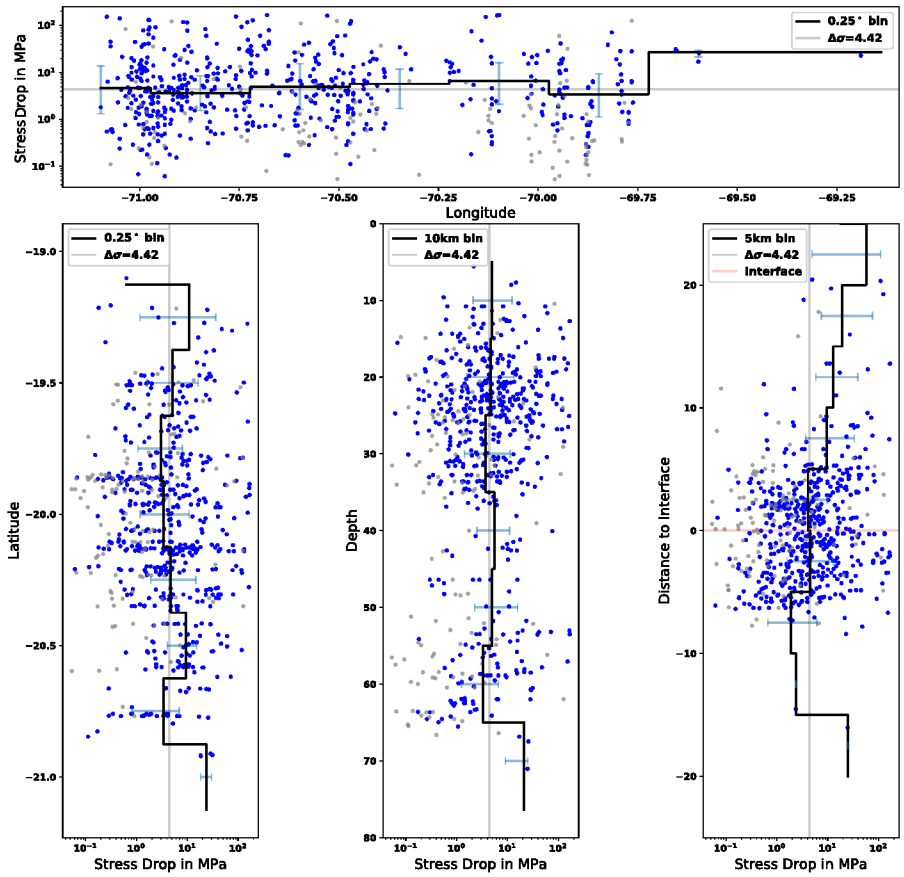

Figure S 26: Stress drop variation in four sections. The figure is similar to Figure 9 in the main manuscript but it shows the corrected stress drop values from Figure S 24. Note that the curves are very similar to those in the original figure but that the overall range of variation is reduced. This indicates that there is stress drop variation and moment variation who both contribute to the resulting stress drop as reported in the original figure.

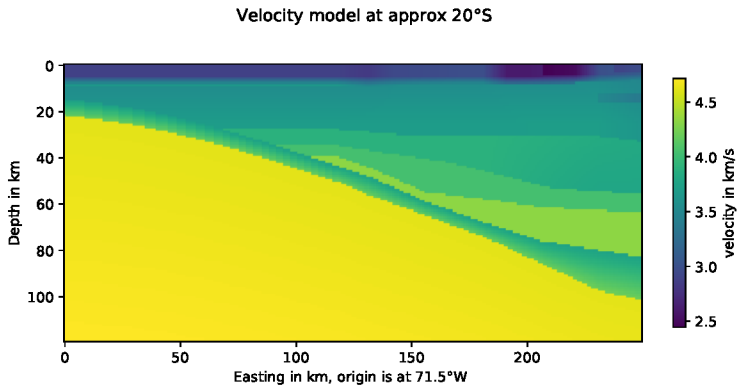

Figure S 27: S phase velocity model slice at 20°S taken from Bloch et al. 2014.

Description of Resulting Stress drop Table

File name: stress_drop_tbl_NChile.txt

Columns are: Event origin time, latitude, longitude, depth, moment magnitude, corner frequency, stress drop, number of contributing data traces, internal ID.

Origin time, latitude, longitude, depth are taken from Sippl et al. 2018.
Moment magnitudes are taken from Münchmeier et al. 2020.

Note that the internal ID can occur twice. First occurrence is the P phase, second is the S phase based estimate.

Important! Note that P phase based stress drops have been computed with k_p=0.32 and S phase based stress drop estimates have been computed with k_s = 0.276, resulting from the empirical k-ratio obtained in Figure 2, main manuscript.
The table contains also stress drops estimates that lie beyond the defined resolution limits (M<2.5 and $1 \leq f_c \leq 20Hz$) which are shown in grey in Figure 11 main manuscript.